Available online at www.sciencedirect.com
SCIENCE DIRECT
Catalysis Today 98 (2004) 141–150
CATALYSIS TODAY
www.elsevier.com/locate/cattod

New NiMo catalysts supported on Al-containing SBA-16 for 4,6-DMDBT hydrodesulfurization Effect of the alumination method

T. Klimova[a,*], L. Lizama[a], J.C. Amezcua[a], P. Roquero[a], E. Terrés[b], J. Navarrete[b], J.M. Domínguez[b]

[a]*Departamento de Ingeniería Química, Facultad de Química, UNAM, Cd. Universitaria, C.P. 04510, Coyoacan, México D.F., México*
[b]*Programa de Ingeniería Molecular, Instituto Mexicano del Petróleo, Eje Central Lázaro Cárdenas # 152, C.P. 07730 México D.F., México*

Abstract

A series of Al-containing mesoporous molecular sieves SBA-16 was prepared by synthetic and post-synthetic methods using different Al sources. NiMo catalysts supported on Al-SBA-16 were prepared and tested in the 4,6-dimethyldibenzothiophene hydrodesulfurization (HDS) reaction. The synthesized solids were characterized by N_2 physisorption, XRD, ammonia TPD, Py FT-IR, ^{27}Al MAS–NMR, temperature programmed reduction, chemical analysis and HRTEM. It was found that the characteristics of the Al-SBA-16-supports strongly depend on the used Al source and the method selected for Al incorporation into the SBA structure. Post-synthetic alumination of SBA-16 by reacting with $AlCl_3$ or Al(i-PrO)$_3$ has a number of advantages in comparison with the incorporation of Al by grafting with $NaAlO_2$ or direct synthesis, among them, (i) a good control of Al content in the sample; (ii) little influence on the mesoporous structure of the parent SBA-16; (iii) creation of Brönsted acid sites; and (iv) stronger interaction with deposited Ni and Mo species providing them better dispersion. NiMo catalysts supported on Al-SBA-16, which were prepared by grafting with $AlCl_3$ or Al(i-PrO)$_3$, show high activity in 4,6-DMDBT HDS; this can be attributed to good dispersion of Ni and Mo active phases and to the bifunctional character of these catalysts, namely, to the participation of both types of sites, coordinatively unsaturated sites (CUS) of NiMoS active phase and Brönsted acid sites of the support, in the catalytic transformations of 4,6-DMDBT.

Keywords: NiMo catalysts; Al-SBA-16; Hydrodesulfurization; 4,6-Dimethyldibenzothiophene; Bifunctional catalysts

1. Introduction

Nowadays, many efforts are aimed to improve the hydrodesulfurization (HDS) catalysts by using new materials as catalytic supports. Mesoporous molecular sieves MCM-41, with mesopores of 20–35 Å in diameter, surface area of 700–1000 m^2/g and intermediate acidity, have attracted much interest in petroleum hydrotreating processes [1–5]. Al-containing mesoporous molecular sieves are particularly attractive as heterogeneous catalysts and sorbents for large organic molecules where microporous zeolites cannot be used. However, MCM-41-type materials have poor stability, which represents a serious limitation to their practical applications [6]. Recently, a novel family of mesoporous silicas (SBA) was synthesized by using neutral organic triblock copolymers [7–10]. This new materials have larger pores, thicker pore walls and higher hydrothermal stability with respect to MCM-41 [7,10–12]. However, the problem of the preparation of Al-containing SBA materials is not completely solved yet. Some authors report that Al-containing SBA-15 can be obtained by direct incorporation of Al into the framework of SBA-15 during the hydrothermal synthesis [13,14]. Others consider that Al could not be incorporated into the SBA structure in these conditions, since most Al sources dissolve in the strong acidic media normally used for the synthesis. Therefore, post-synthetic grafting of Al^{3+} onto SBA-15 surface seems to be more recommended [15,16]. It was reported that the latter materials had superior structural integrity, acidity and catalytic activity to those of materials

* Corresponding author. Tel.: +52 55 56225371; fax: +52 55 56225371.
E-mail address: klimova@servidor.unam.mx (T. Klimova).

0920-5861/$ – see front matter © 2004 Elsevier B.V. All rights reserved.
doi:10.1016/j.cattod.2004.07.028

having Al incorporated during synthesis. To clarify this controversy, in this work four samples of mesoporous Al-SBA-16 were synthesized by known, synthetic and post-synthetic, procedures and tested as supports for NiMo HDS catalysts. The aim of the present work is to study the efficiency of the different methods of preparation of Al-SBA-16 and their effect on the characteristics of the Al-containing SBA-supports, corresponding NiMo catalysts and the performance of the last ones in the 4,6-dimethyldibenzothiophene (4,6-DMDBT) HDS reaction.

2. Experimental

2.1. Support and catalyst preparation

The pure siliceous cubic *Im* $\bar{3}m$ SBA-16 (Si-SBA-16 sample) was prepared according to the literature [17,18] using the triblock copolymer Pluronic F127 ($EO_{106}PO_{70}$-EO_{106}, BASF) as the structure-directing agent and tetraethyl orthosilicate (TEOS) as the silica source. Four grams of Pluronic F127 was dissolved in 30 g of water and 120 g of 2 M HCl solution at 35 °C. Then 8.50 g of TEOS was added into the solution. The mixture was stirred at 35 °C for 20 h and then aged at 100 °C for 72 h without stirring. The solid product was recovered by filtration, washed with deionized water, and air-dried at room temperature. Calcination was carried out in static air at 550 °C for 6 h. This silica SBA-16 was used as a parent material to produce Al-containing SBA-16 via post-synthetic alumination. A detailed synthesis procedure is reported in [16]. Three different Al sources were used for post-synthetic alumination procedure: $AlCl_3$ in dry ethanol (Al-SBA-16(I) sample), Al(i-PrO)$_3$ in hexane (Al-SBA-16(II) sample), and sodium aluminate in aqueous solution (Al-SBA-16(III)). A typical synthetic procedure was as follows: 1 g of Si-SBA-16 was combined with 100 ml of dry ethanol containing the required amount of $AlCl_3$. This mixture was kept with magnetic stirring at room temperature for 12 h. The solid material was then filtered, washed vigorously with dry ethanol, dried at room temperature in air and calcined in static air at 550 °C for 5 h. Additionally, one Al-containing sample was prepared by direct synthesis (Al-SBA-16(DS)) as it is described in [13]. In this case, aluminum isopropoxide and TEOS were added to 10 mL of aqueous HCl at pH 1.5. After stirring for 3 h this solution was added to a second solution containing 4 g of Pluronic F127 in aqueous HCl at pH 1.5 at 30 °C. This mixture was stirred for another 1 h and allowed to react at 100 °C for 24 h. In all the cases Si/Al ratio during the preparation was preserved equal to 30.

NiMo/SBA-16 catalysts were prepared by a standard incipient wetness technique. The calcined supports were impregnated successively using aqueous solutions of ammonium heptamolybdate and nickel nitrate. Mo was impregnated first. After each impregnation, the catalysts were dried (100 °C, 24 h) and calcined (500 °C, 2 h). The nominal composition of the catalysts was 12 wt.% of MoO_3 and 3 wt.% of NiO.

2.2. Support and catalyst characterization

The supports and catalysts were characterized by N_2 physisorption, XRD, chemical analysis, HRTEM, ammonia TPD, Py FT-IR, temperature programmed reduction (TPR), and ^{27}Al MAS–NMR. N_2 adsorption/desorption isotherms were measured with a Micromeritics ASAP 2000 automatic analyzer at liquid N_2 temperature. Prior to the experiments, the samples were degassed ($P < 10^{-1}$ Pa) at 270 °C for 6 h. Specific surface areas were calculated by the BET method (S_{BET}), the pore volume (V_p) was determined by nitrogen adsorption at a relative pressure of 0.98 and pore size distributions from the adsorption isotherms by the BJH method. The microporous area was estimated using the correlation of t-Harkins and Jura (t-plot method). XRD patterns were recorded in the $3^\circ \leq 2\Theta \leq 90^\circ$ range in a Siemens D5000 diffractometer, using Cu K_α radiation (λ = 1.5406 Å) and a goniometer speed of $1^\circ(2\Theta)$ min^{-1}. Small-angle XRD (2Θ = 1–10°) was performed on the Bruker D8 Advance diffractometer using small divergence and scattering slits of 0.05°. NH_3 TPD and TPR experiments were carried out in an automated ISRI-RIG-100 characterization system equipped with a TC detector. Before ammonia adsorption, the samples were pretreated at 500 °C, 1 h in air flow and 1 h in helium flow, in order to remove water and other contaminants. The samples were then cooled to room temperature and contacted with a He/NH_3 mixture (90/10 v/v) at a flow rate of 30 ml min^{-1} for 1 h. The desorption step was performed in He stream (20 ml min^{-1}) with a heating rate of 5 °C/min. After reaching 500 °C the sample was kept at this temperature until the trace reached the base line. In the TPR experiments, the samples were pretreated in situ at 500° for 2 h under air flow and cooled in an Ar stream. The reduction step was performed with an Ar/H_2 mixture, with a heating rate of 10 °C/min, up to 1000 °C. IR spectra of the supports were recorded in a transmittance mode with a Nicolet Magna 750 Fourier transform spectrometer, with a resolution of 4 cm^{-1}, and 200 scans. The samples were prepared as self-supporting wafers by pressing and were loaded on a sample holder of the IR cell. After the sample was evacuated at 10^{-4} Torr at 400 °C for 2 h and then cooled to room temperature in vacuo, the IR spectra of the calcined state were recorded. Pyridine was adsorbed on the wafer at room temperature and evacuated and heated at various temperatures. Solid state ^{27}Al MAS–NMR spectra were obtained with a ASX300 Bruker NMR spectrometer using $Al(H_2O)_6^{3+}$ as an external ^{27}Al reference. The spectra were recorded at 25 °C, at a source frequency of 78.210 MHz and a spinning rate of 12 KHz with radio frequency pulses of 2.0 μs. The NMR spectra were obtained for dry and hydrated samples. Dry samples were prepared by thermal treatment at 100 °C for 72 h previous to NMR data acquisition. To obtain hydrated samples, Al-SBA-16-

supports were kept in water-saturated atmosphere for 72 h. High resolution transmission electron microscopy (HRTEM) studies were performed using a Jeol 2010 microscope (resolving power 1.9 Å). The solids were ultrasonically dispersed in heptane and the suspension was collected on carbon coated grids. Slab length and layer stacking distributions of MoS_2 crystallites in each sample were established from the measurement of at least 300 crystallites detected on several HRTEM pictures taken from different parts of the same sample dispersed on the microscope grid. The chemical analysis of the supports and NiMo catalysts was made by Desert Analytics (USA).

2.3. Catalytic activities

The 4,6-DMDBT HDS activity tests were performed in a batch reactor at 300 °C and 7.3 MPa total pressure for 8 h. Prior to the catalytic activity tests, the catalysts were sulfided ex situ in a tubular reactor at 400 °C for 4 h in a stream of 15 vol.% of H_2S in H_2 under atmospheric pressure. The course of the reaction was followed by taking liquid samples each hour and analyzing them in an HP-6890 chromatograph. To corroborate product identification, the product mixture was analyzed in a Hewlett Packard GC-MS equipment.

3. Results and discussion

3.1. Supports

The chemical compositions of the synthesized SBA-16 molecular sieves are given in Table 1. The results from chemical analysis show that Si/Al molar ratio in the materials prepared by different post-synthetic procedures are in close agreement with the calculated value Si/Al = 30. This means that the aluminum has been mostly incorporated into the siliceous SBA-16. The Si/Al ratio found for the sample prepared by direct synthesis (Al-SBA-16(DS)) was substantially higher (at about 254) indicating that in this case only a small part of Al atoms was incorporated into the SBA-16 framework, probably, due to strong acidic media used in the synthesis.

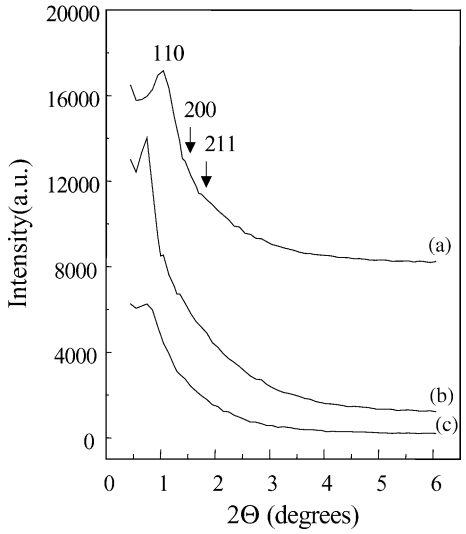

Fig. 1. Powder X-ray diffraction patterns of Si-SBA-16 (a) and Al-SBA-16(DS) (b) supports; and NiMo/Al-SBA-16(DS) catalyst (c).

The purely siliceous parent SBA-16 was prepared according to the previously described procedure [17,18], using a stirring time of 20 h at 35 °C, followed by an aging period of 72 h at 100 °C. The XRD pattern of this calcined sample (Fig. 1a) shows a very strong (1 1 0) reflection (1.05° 2Θ) of the cubic *Im* $\bar{3}m$ structure and two small shoulders of the (2 0 0) and (2 1 1) reflections (1.43 and 1.75° 2Θ, respectively). All these reflections yield an a_o value of 124 Å, confirming that the measured structure is indeed the *Im* $\bar{3}m$ structure [10,18]. Similar XRD pattern was also observed for the Al-SBA-16(DS) sample (Fig. 1b). However, in this case the positions of (1 1 0), (2 0 0) and (2 1 1) reflections were shifted to 0.80, 1.14 and 1.39° 2Θ, respectively, giving a_o a value of 156 Å. In the preparation of this sample we followed the methodology reported in [13] in order to achieve the direct incorporation of Al species into the SBA-16 structure during the hydrothermal synthesis of the mesostructured material. In particular, the order of mixing of the reactants, stirring and aging regime were different in comparison with the used in the synthesis of the previously described Si-SBA-16. Therefore, the observed differences in XRD patterns of these two samples can be attributed to the differences in the preparation procedure used in both cases.

Table 1
Textural characteristics and chemical compositions of SBA-16 molecular sieves

Sample	Al^{3+} source	Si/Al molar ratio	S_{BET} (m^2/g)	V_p (cm^3/g)	D_p[a] (Å)	S_μ[b] (m^2/g)	V_μ[c] (cm^3/g)
Parent Si-SBA-16	–	–	817	1.091	65	50	0.013
Al-SBA-16(I)	$AlCl_3$	29.5	746	1.013	64	51	0.014
Al-SBA-16(II)	Al(i-PrO)$_3$	30.5	789	1.082	64	49	0.013
Al-SBA-16(III)	$NaAlO_2$	30.0	442	0.793	62	21	0.004
Al-SBA-16(DS)	Al(i-PrO)$_3$	254	936	0.604	50	107	0.039

[a] Pore diameter determined from the adsorption isotherms by the BJH method.
[b] Micropore area.
[c] Micropore volume.

Nitrogen adsorption–desorption isotherms of the parent Si-SBA-16 and Al-SBA-16(DS) samples are shown in Figs. 2 and 3. The very typical adsorption–desorption hysteresis, characteristic for ink-bottle pores of SBA-16 material, is clearly observed for both samples. The pore size distributions, calculated from the adsorption branch of the isotherms, show a narrow distribution of mesopores, distributed around an average pore diameter of 65 Å for Si-SBA-16 sample and around 50 Å for Al-SBA-16(DS). The pore wall thickness (h_w) of Si-SBA-16 and Al-SBA-16 (DS) materials was calculated from a simple formula $h_w = \sqrt{3}a_o/2 - D_p$, where D_p and a_o are the mesopore diameter and cubic unit cell parameter, respectively [18]. It was found that the walls of Al-SBA-16(DS) are of about two times thicker than of the Si-SBA-16 counterpart (85 Å versus 42 Å, respectively).

Nitrogen adsorption–desorption isotherms from the aluminum-containing SBA-16 materials prepared via post-synthetic procedure are shown in Fig. 3. The shape of the adsorption isotherms the Al-SBA-16 samples prepared by reacting Si-SBA-16 with $AlCl_3$ or $Al(i\text{-}PrO)_3$ is similar to that of the parent siliceous SBA-16, indicating that post-synthetic alumination with these aluminum sources does not affect the original pore structure of the parent material. However, the use of $NaAlO_2$ aqueous solution in the post-synthetic alumination produces a significant decrease in the amount of the adsorbed N_2, reflecting a drop in surface area and total pore volume. This suggests partial destruction of the pore arrangement and the possible existence of some amorphous domains in the Al-SBA-16(III) sample.

In line with previously reported results [11,18,19], all SBA-16 materials synthesized in the present work, purely siliceous and Al-containing, have the combined micro- and mesoporosity (Table 1). The comparison of the ratio micropores/mesopores of two samples, parent Si-SBA-16 and Al-SBA-16(DS), shows that last material has the highest

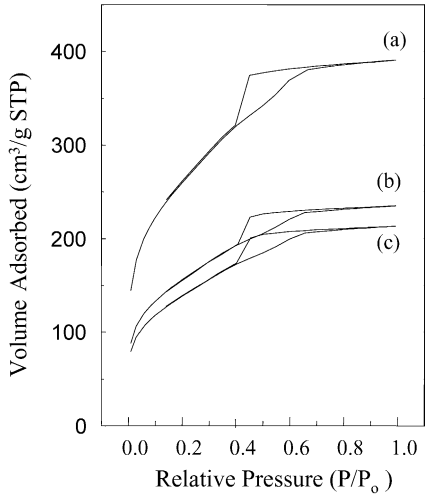

Fig. 2. Nitrogen adsorption–desorption isotherms of Al-SBA-16(DS)-support (a); Mo/Al-SBA-16(DS) (b); and NiMo/Al-SBA-16(DS) (c) catalysts.

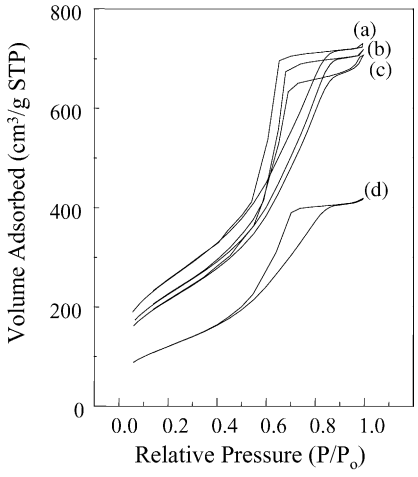

Fig. 3. Nitrogen adsorption–desorption isotherms of the parent Si-SBA-16 (a) and Al-containing supports prepared via post-synthetic alumination: (b) Al-SBA-16(II); (c) Al-SBA-16(I); and (d) Al-SBA-16(III).

proportion of micropores, that can be attributed to the shorter time of its hydrothermal synthesis (24 h) in comparison with the time used in the preparation of the purely siliceous counterpart (72 h). The textural characteristics of the Al-containing SBA-16-supports prepared by grafting strongly depend on the aluminum source used in the preparation. From Table 1, it is possible to see, that post-synthetic alumination of SBA-16 by reacting with $AlCl_3$ or $Al(i\text{-}PrO)_3$ leads only to a slight decrease of surface area and total pore volume comparing with the parent material. In contrast, alumination with $NaAlO_2$ aqueous solution reduces significantly the surface area and pore volume and narrows the pore diameter of the parent Si-SBA-16. Observed degradation of the structure of the siliceous SBA-16 probably is induced by the presence of sodium hydroxide in the impregnation solution of $NaAlO_2$. Different types of possible pathogenic reactions between NaOH and silica are well known from the literature [20].

^{27}Al MAS–NMR results show that the alumination procedure has also a strong effect on the Al coordination (Figs. 4 and 5) Two types of lines can be observed in ^{27}Al MAS–NMR spectra. The chemical shift at 53 ppm can be assigned to aluminum in a tetrahedral environment (AlO_4 structural unit, Al(tet)), in which aluminum is covalently bound to four Si atoms via oxygen bridges. The line at 0 ppm can be assigned to octahedral aluminum (AlO_6 structural unit, Al(oct)) [21]. The results clearly show the simultaneous presence of both tetrahedral and octahedral Al species in the spectra of dry and hydrated Al-SBA-16(I) and Al-SBA-16(II) samples produced by reacting siliceous SBA-16 with $AlCl_3$ or $Al(i\text{-}PrO)_3$, respectively. The 0 ppm signal is more intense in the spectra of both, dry and hydrated, Al-SBA-16(II) sample, this indicates that a lower proportion of aluminum is incorporated into SBA-16 framework via alumination with $Al(i\text{-}PrO)_3$. In contrast, the ^{27}Al MAS–NMR spectra of dry and hydrated Al-SBA-16(III), prepared using sodium aluminate solution, shows only one line at

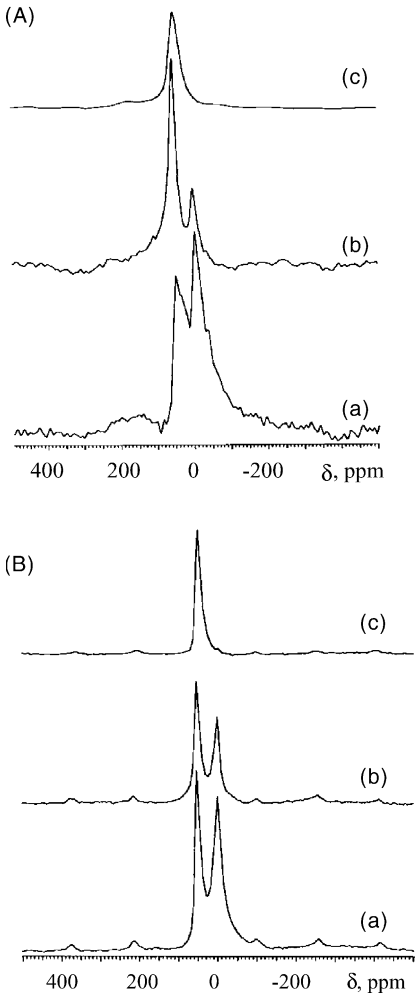

Fig. 4. ^{27}Al MAS–NMR spectra of dry (A) and hydrated (B) Al-containing SBA-16 samples: (a) Al-SBA-16(II); (b) Al-SBA-16(I); and (c) Al-SBA-16(III).

53 ppm indicating that in this case all aluminum has been incorporated into the siliceous framework of parent SBA-16 material. Therefore, it can be concluded that for the samples prepared via post-synthetic Al grafting, the percentage of tetrahedral framework Al species is decreasing in the following order: Al-SBA-16(III) > Al-SBA-16(I) > Al-SBA-16(II). This result is in excellent agreement with previous report [16], where the same distribution of tetrahedral and octahedral Al species was obtained for other SBA-type material, SBA-15, when aluminum was

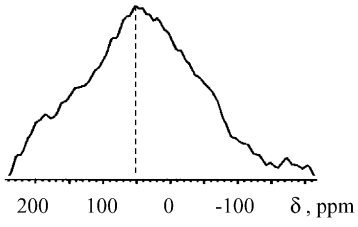

Fig. 5. ^{27}Al MAS–NMR spectrum of dry Al-SBA-16(DS) sample.

incorporated by post-synthetic grafting procedure using different Al sources. It seems that the proportion of framework and extra-framework Al species in different types of SBA materials prepared by post-synthetic Al incorporation is rather determined by the aluminum source and the solvent used in the preparation than by the type of the SBA sieve. The spectrum of dry Al-SBA-16(DS) sample (Fig. 5) shows a very broad and poorly resolved peak with a maximum at around 53 ppm caused by distribution of different environments of the Al nuclei in the solid.

Fig. 6 shows the NH_3 TPD traces of the SBA-16-supports normalized per square meter of surface. It is possible to see in this figure that parent Si-SBA-16 and Al-SBA-16(DS) show only one well-defined peak at 80–150 °C related to very weak interaction of ammonia with silica surface. Incorporation of aluminum in SBA-16 by grafting procedure leads to an increase in the population of acid sites. In fact, we observe an increase in the number of all types of acid sites, but especially of weak and medium (temperature of ammonia desorption between 150 and 350 °C) ones. In line with this, the results of the quantitative evaluation of acid sites (Table 2) indicate that the total density of acid sites of all Al-containing SBA-16 prepared by post-synthetic methods are substantially higher than of parent Si-SBA-16. Py FT-IR (Table 2) clearly shows the appearance of Brönsted acidity in the Al-SBA-16(I) and Al-SBA-16(II) samples induced by the tetrahedral framework Al atoms in the structure. However, the results obtained in FT-IR measurements of adsorbed Py after evacuation at different temperatures reveal that only a half of these Brönsted acidic sites, or less, still remain after heating and evacuating the samples at 300 °C. Unexpectedly, Brönsted acidic sites were not detected in Al-SBA-16(III) sample with the highest proportion of tetrahedral Al species (almost 100%). This is probably due to the presence of Na^+ cations, which balance

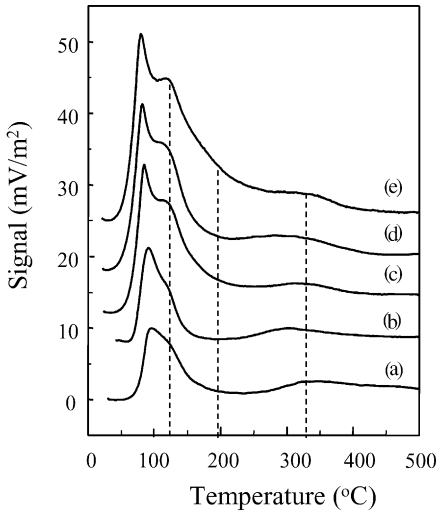

Fig. 6. Ammonia TPD thermograms of SBA-16-supports: Si-SBA-16 (a); Al-SBA-16(DS) (b); Al-SBA-16(I) (c); Al-SBA-16(II) (d); and Al-SBA-16(III) (e).

Table 2
Surface acidity of SBA-16 molecular sieves determined by NH_3 TPD and Py FT-IR

Sample	TPDA (μmol)		Py FT-IR (μmol Py/g)								
	NH_3/m^2	NH_3/g	Brönsted			Lewis			Total		
			100[a]	200	300	100	200	300	100	200	300
Si-SBA-16	3.9	3146	–	–	–	–	–	–	–	–	–
Al-SBA-16(I)	8.5	6114	63	57	35	164	63	41	227	120	76
Al-SBA-16(II)	9.1	7154	91	64	35	256	75	62	347	139	97
Al-SBA-16(III)	9.9	4400	0	0	0	169	11	0	169	11	0
Al-SBA-16(DS)	3.4	3486	0	0	0	102	26	0	102	26	0

[a] Temperature of Py desorption (°C).

the negative charges associated with tetrahedral aluminums incorporated into the siliceous framework.

3.2. Catalysts

Chemical analysis results show that the actual chemical composition (Ni and Mo loading) of all the prepared NiMo catalysts is close to the expected nominal one, 12 wt.% of MoO_3 and 3 wt.% of NiO (Table 3). The textural characteristics of NiMo catalysts supported on SBA-16 molecular sieves are given in Table 3. A significant decrease in surface area and pore volume is observed when Ni and Mo are incorporated to the support. This decrease is more pronounced for the catalysts supported on Al-SBA-16(DS), support with small pores and low aluminum loading, and on the support aluminated with $NaAlO_2$ solution.

Fig. 2 shows the changes in the nitrogen adsorption–desorption isotherms after successive incorporation of Mo and Ni species to the Al-SBA-16(DS)-support. A significant decrease in the amount of the adsorbed nitrogen is observed after metal impregnation, especially after Mo deposition. However, the hysteresis loop maintains its shape characteristic for SBA-16 structure. In line with this, a characteristic (1 1 0) reflection of *Im* $\bar{3}m$ structure is still observed in the XRD pattern of NiMo/Al-SBA-16(DS) catalyst (Fig. 1c). However, a significant decrease in its intensity and broadening after Ni and Mo deposition suggests some loss in the periodicity of the Al-SBA-16(DS) pore structure. Therefore, a strong obstruction of the support pores after metal deposition could be supposed to occur in this catalyst.

The incorporation of Al atoms in the SBA-16-support via post-synthetic alumination with $AlCl_3$ or $Al(i\text{-}PrO)_3$ seems to improve the catalyst textural characteristics (Table 3). Additionally, a small reduction of pore size (from 64 to 60 Å) is observed in all NiMo catalysts supported on Al-SBA-16 materials prepared by post-synthetic grafting of aluminum species, this suggests that the deposited Mo and Ni oxide species are located inside the pores of Al-SBA-16-support.

Powder XRD patterns for NiMo catalysts supported on different SBA-16-type materials are shown in Fig. 7. It should be mentioned that the XRD patterns of the SBA-16-supports did not show the presence of any crystalline phase. In the case of NiMo catalysts, diffraction lines corresponding to reflections of MoO_3 in orthorhombic phase (JCPDS

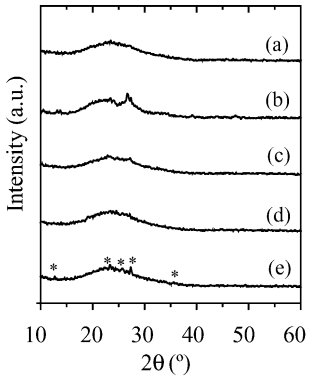

Fig. 7. XRD patterns of NiMo catalysts supported on Si-SBA-16 (a); Al-SBA-16(III) (b); Al-SBA-16(II) (c); Al-SBA-16(I) (d); and Al-SBA-16(DS) (e). (*) MoO_3, JCPDS card 35-609.

Table 3
Actual compositions and textural characteristics of NiMo catalysts supported on SBA-16-type supports

Sample	Chemical composition[a] (wt.%)				S_{BET} (m^2/g)	V_p (cm^3/g)	D_p[b] (Å)
	NiO	MoO_3	SiO_2	Al_2O_3			
NiMo/Si-SBA-16	2.95	12.10	84.95	0	495	0.636	65
NiMo/Al-SBA-16(I)	2.98	12.20	82.44	2.38	536	0.726	60
NiMo/Al-SBA-16(II)	3.05	12.25	82.40	2.30	476	0.693	60
NiMo/Al-SBA-16(III)	2.90	11.95	82.80	2.35	230	0.452	60
NiMo/Al-SBA-16(DS)	2.93	12.02	84.77	0.28	498	0.330	48

[a] Determined by chemical analysis.
[b] Pore diameter determined from the adsorption isotherms by the BJH method.

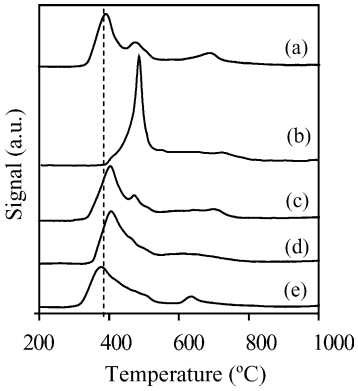

Fig. 8. TPR profiles for NiMo catalysts supported on Si-SBA-16 (a); Al-SBA-16(III) (b); Al-SBA-16(II) (c); Al-SBA-16(I) (d); and Al-SBA-16(DS) (e).

card 35–609) are observed only for NiMo catalyst supported on Al-SBA-16(DS), this may be due to low aluminum content and small pore diameter of this support. Interestingly, a group of new peaks located between 25° and 30° 2Θ is observed in the XRD pattern of NiMo/Al-SBA-16(III) catalyst. The appearance of these signals makes evident that the formation of a mixture of different crystalline phases, such as aluminum silicate (JCPDS card 25-0021), sodium hydrogen silicate hydrate (JCPDS card 29–1212) and zeolite ZSM-5 (JCPDS card 40-0064), takes place in this sample after Ni and Mo deposition and following calcination.

The TPR results for NiMo/SBA-16 catalysts are shown in Fig. 8. The TPR profile of the NiMo/Si-SBA-16 sample exhibits three main reduction peaks at 392, 476 and 689 °C. The low temperature peak (392 °C) is associated generally to the reduction of Mo^{6+} to Mo^{4+} of polymeric octahedral Mo species weakly bound to the silica surface (probably small clusters of MoO_3, not detected by XRD) [22,23]. Comparing the present TPR pattern with TPR of $NiMoO_4$ (main peak at 475 °C) [24], the second reduction peak may be assigned to a formation of a $NiMoO_4$-like phase. Finally, the peak at about 690 °C in the case of SiO_2-supported Mo catalysts is ascribed to the second step of reduction of the MoO_3 species [23]. The TPR characterization of NiMo catalysts supported on Al-containing SBA-16 (Fig. 8) shows that post-synthetic Al incorporation into the SBA leads to an increase in the temperature of Ni and Mo reduction because of their stronger interaction with the Al-containing support. However, alumination by reacting SBA-16 with $NaAlO_2$ results in a significant increase in the proportion of Ni and Mo species difficult to reduce (main reduction peak at 488 °C). In the case of Al-SBA-16(DS)-support, the interaction with NiMo oxide species is not so strong, and the reduction of the octahedral Mo species takes place at about 380 °C.

Additional information can be obtained from the analysis of the shape of the obtained TPR patterns. Previously, it was observed for MoO_3/SiO_2 catalysts that the broadness of the low temperature peak is related with the dispersion of Mo species, namely, broad TPR peaks are often observed for monolayer-type (dispersed) catalysts, whereas bulk compounds in general show sharp TPR signals [25]. From this point of view, it can be expected that, in our case, NiMo catalysts supported on Al-containing SBA-16, with the exception of Al-SBA-16(III)-support, should have better dispersed metal oxide species than those supported on parent Si-SBA-16 material.

These suggested changes in the morphology of Mo species were corroborated by HRTEM observations of the sulfided catalysts. The micrographs show the typical fringes due to MoS_2 crystallites with 6.2 Å interplanar distances (Fig. 9). It can be observed that the morphology of MoS_2 crystallites, namely, the number of stacked layers and their length, changes depending on the support. In the Si-SBA-16-supported catalyst, MoS_2 crystallites with length between 20 and 60 Å and stacking from two to four layers are found (Fig. 9a). Aluminum incorporation into the framework of SBA-16 material during its hydrothermal synthesis (Al-SBA-16(DS)) almost does not affect the slab length but results in a slight decrease in stacking degree of MoS_2 active phase. In contrast, post-synthetic alumination of SBA-16 surface leads to a substantial decrease in length and stacking of the MoS_2 structures (Fig. 9b). The distributions in stacking degree and slab length for different catalysts are presented in Fig. 10. The best dispersion of MoS_2 crystallites, shorter length and single or double stacked slabs, is observed in the catalyst supported on Al-SBA-16 material aluminated by grafting with $Al(i\text{-}PrO)_3$ in hexane.

3.3. Catalytic activity

In the present study, the catalytic activity of sulfided NiMo/SBA-16 catalysts was examined in the hydrodesulfurization of 4,6-dimethyldibenzothiophene, one of the most refractory sulfur compounds in gas oil [26]. The conversion of 4,6-DMDBT is shown in Table 4 and Fig. 11. It can be observed that 4,6-DMDBT conversion reached at 8 h is changed in a wide range. Thus, high catalytic activity (66–67% of 4,6-DMDBT conversion) is reached for the catalysts supported on Al-SBA-16(I) and Al-SBA-16(II). Catalytic activities of NiMo catalysts supported on parent siliceous Si-SBA-16 and Al-containing support prepared by direct synthesis are slightly lower (50 and 47% of 4,6-DMDBT conversion, respectively). NiMo/Al-SBA-16(III) catalyst leads to the lowest 4,6-DMDBT conversion (23%). This activity trend with the change of the Al-containing SBA-16-support would be the result of two opposite effects: on one hand, the incorporation of aluminum onto the support surface provides a stronger metal-support interaction, allowing a better dispersion of the molybdenum and nickel oxidic and sulfided phases. On the other hand, too strong metal-support interaction, as in the case on NiMo/Al-SBA-16(III) catalyst, makes the reduction and sulfidation of Ni and Mo species more difficult. As it is shown above, the characteristics of Al-containing SBA-supports and corresponding NiMo catalysts strongly depend on the method of

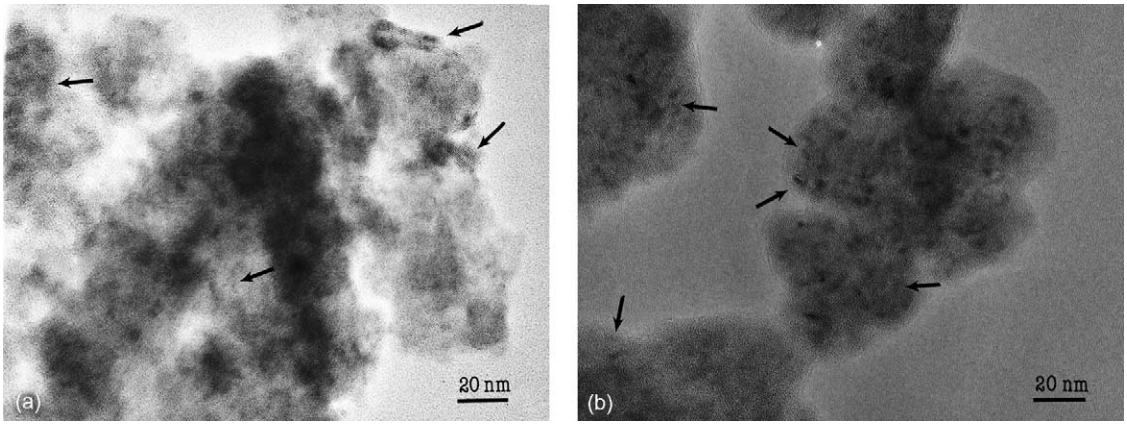

Fig. 9. HRTEM micrographs for sulfided catalysts: NiMo/Si-SBA-16 (a); and NiMo/Al-SBA-16(I) (b).

preparation of the Al-SBA-16-support and the Al source used. This evidences that only the Al-SBA-16-supports prepared by post-synthetic aluminum grafting with $AlCl_3$ in dry ethanol or $Al(i\text{-}PrO)_3$ in hexane have appropriate characteristics to be used as catalytic-supports for NiMo catalysts for HDS of refractory dibenzothiophenes.

Nowadays, it is known that the HDS of methyl-substituted DBT derivatives occurs through two parallel reactions, namely, (i) direct desulfurization (DDS) yielding corresponding substituted biphenyl (BP) products, and (ii) hydrogenation with subsequent desulfurization (HYD), yielding first substituted tetrahydrodibenzothiophenes, then corresponding hexahydro-derivatives, and finally, cyclohexylbenzene-type compounds [27,28]. To elucidate the influence of the difference of supports on the reaction pathways of 4,6-dimethyldibenzothiophene, the reaction product distributions at the same total 4,6-DMDBT conversion (20%) was compared for different catalysts (Table 4). The detailed analysis of the reaction products show that for all SBA-16-supported catalysts the preferential pathway is HYD. When Al-atoms are incorporated into the SBA-16-support, the proportion of HYD route products

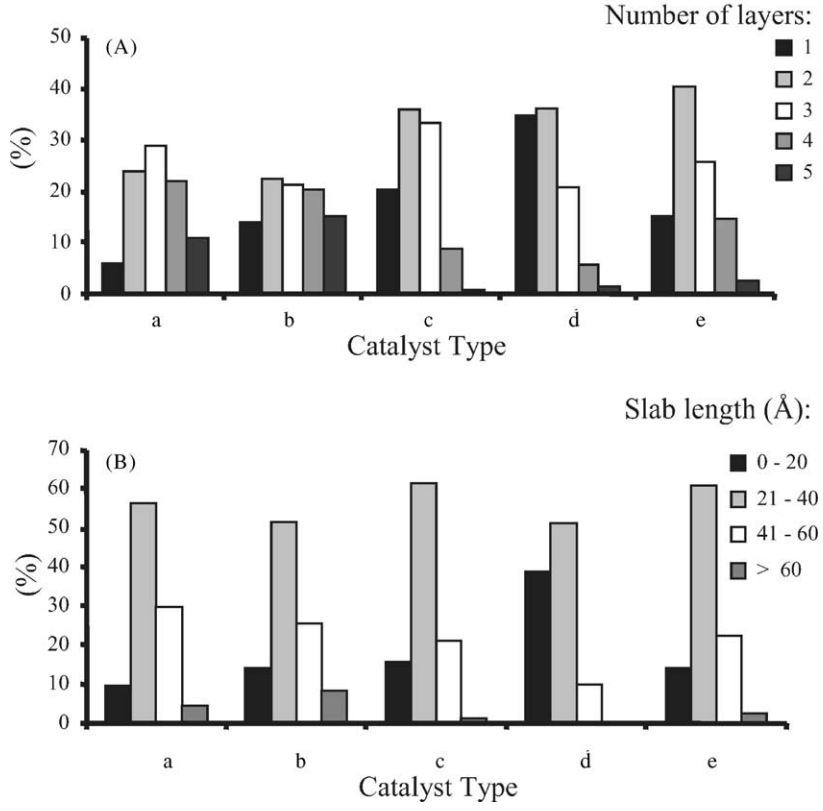

Fig. 10. Layer stacking (A) and length (B) distribution of MoS_2 crystallites in sulfided NiMo catalysts supported on Si-SBA-16 (a); Al-SBA-16(III) (b); Al-SBA-16(II) (c); Al-SBA-16(I) (d); and Al-SBA-16(DS) (e).

Table 4
4,6-DMDBT conversions and reaction product compositions obtained over NiMo/SBA-16 catalysts

Catalyst	4,6-DMDBT conversion[a] (%)	Product composition[b] (%)				HYD/DDS ratio[b]
		THDMDBT	HHDMDBT	MCHT	DMBP	
NiMo/Si-SBA-16	50.0	36.4	10.7	42.1	10.8	8.26
NiMo/Al-SBA-16(I)	66.8	33.5	8.0	40.7	17.8	4.62
NiMo/Al-SBA-16(II)	65.7	38.9	10.8	31.3	19.0	4.26
NiMo/Al-SBA-16(III)	23.0	40.9	8.7	33.7	16.7	4.99
NiMo/Al-SBA-16(DS)	47.4	28.7	6.5	51.5	13.3	6.52

[a] At 8 h reaction time.
[b] Determined at 20% of total 4,6-DMDBT conversion. DDS, direct desulfurization pathway; HYD, hydrogenation pathway; THDMDBT, tetrahydrodimethyldibenzothiophene; HHDMDBT, hexahydrodimethyldibenzothiophene; MCHT, methylcyclohexyltoluene; DMBP, dimethylbiphenyl. HYD/DDS pathway ratio was determined as the ratio of HYD route products (THDMDBT + HHDMDBT + MCHT) to DDS route product (DMBP).

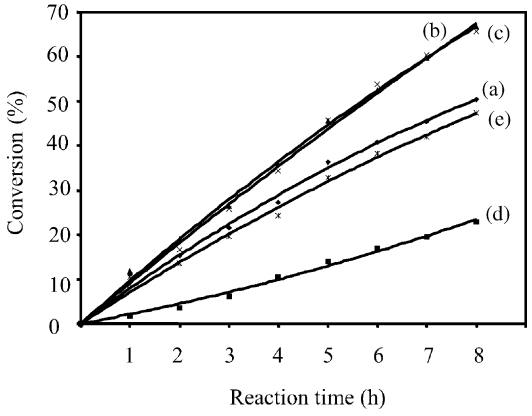

Fig. 11. 4,6-Dimethyldibenzothiophene (4,6-DMDBT) conversions obtained over NiMo catalysts supported on Si-SBA-16 (a); Al-SBA-16(I) (b); Al-SBA-16(II) (c); Al-SBA-16(III) (d); and Al-SBA-16(DS) (e).

decreases, probably, because of better dispersion of MoS_2 active phase. Additionally, for the NiMo catalysts supported on Al-SBA-16(I) and Al-SBA-16(II)-supports with Brönsted acidity it was observed the formation of different isomers of the principal reaction products, dimethylbiphenyl and methylcyclohexyltoluene. This points out the bifunctional character of these active catalysts. Both types of sites, CUS of NiMoS active phase and Brönsted acidic protons of the support, participate in the catalytic transformations of 4,6-DMDBT. First, the Brönsted acid sites isomerize the 4,6-DMDBT changing the position of the methyl substituents in the molecule. This reduces the steric hindrance of methyl groups and makes the following desulfurization more facile. Therefore, high catalytic performance of these catalysts in HDS of refractory DBTs can be attributed to the synergism between both types of active sites.

4. Conclusions

According to the above results, the following conclusions can be stated.

Al-containing SBA-16 can be prepared by synthetic and post-synthetic methods using different Al sources. However, the characteristics of the Al-SBA-16-supports changes depending on the used Al source and the method of Al incorporation into the SBA structure. Our results show that post-synthetic alumination of SBA-16 reacting with $AlCl_3$ or $Al(i\text{-}PrO)_3$ has a number of advantages in comparison with the incorporation of Al by grafting with $NaAlO_2$ or direct synthesis, among them, (i) a good control of Al content in the sample; (ii) little influence on the mesoporous structure of the parent SBA-16; and (iii) creation of Brönsted acid sites.

The interaction of Ni and Mo species with the support becomes stronger with Al loading into the SBA-16 by post-synthetic aluminum grafting. According to this, the dispersion of sulfided Mo species increases. However, when SBA-16 is aluminated using $NaAlO_2$, NiMo catalysts with low surface area and activity are obtained. This points out the method of incorporation of Aluminum into the SBA-type materials and Al sources suitable for the preparation of supports for HDS catalysts.

NiMo catalysts supported on Al-containing SBA-16 molecular sieves, which were prepared by grafting with $AlCl_3$ or $Al(i\text{-}PrO)_3$, show high activity in HDS of refractory dibenzothiophenes (4,6-DMDBT). This can be attributed to good dispersion of Ni and Mo active phases and to the bifunctional character of these catalysts, namely, to the participation of both types of sites: active sites of NiMoS phase and Brönsted acid sites of the support in the catalytic transformations of 4,6-DMDBT.

Acknowledgements

Financial support by DGAPA-UNAM (grant IN-103102) is gratefully acknowledged. The authors wish to thank Ivan Puente, Cecilia Salcedo and Manuel Aguilar-Franco for technical assistance with HRTEM and XRD characterizations.

References

[1] A. Wang, Y. Wang, T. Kabe, Y. Chen, A. Ishihara, W. Qian, J. Catal. 199 (2001) 19.
[2] A. Wang, Y. Wang, T. Kabe, Y. Chen, A. Ishihara, W. Qian, P. Yao, J. Catal. 210 (2002) 319.

[3] T. Klimova, M. Calderón, J. Ramírez, Appl. Catal. A: Gen. 240 (2003) 29.
[4] C. Song, K.M. Reddy, Appl. Catal. A: Gen. 176 (1999) 1.
[5] L. Kaluza, M. Zdrazil, N. Zilkova, J. Cejka, Catal. Comm. 3 (2002) 151.
[6] P.J. Kooyman, P. Waller, A.D. van Langeveld, C. Song, K.M. Reddy, J.A.R. van Veen, Catal. Lett. 90 (2003) 131.
[7] D. Zhao, J. Feng, Q. Huo, N. Melosh, G.H. Fredrickson, B.F. Chmelka, G.D. Stucky, Science 279 (1998) 548.
[8] D. Zhao, Q. Huo, J. Feng, B.F. Chmelka, G.D. Stucky, J. Am. Chem. Soc. 120 (1998) 6024.
[9] C. Göltner-Spickermann, Curr. Opin. Interf. Coll. Sci. 7 (2002) 173.
[10] C.-F. Cheng, Y.-C. Lin, H.-H. Cheng, Y.-C. Chen, Chem. Phys. Lett. 382 (2003) 496.
[11] A. Galarneau, H. Cambon, F. Di Renzo, F. Fajula, Langmuir 17 (2001) 8328.
[12] Y. Bennandja, P. Beaunier, D. Margolese, A. Davidson, Micropor. Mesopor. Mater. 44–45 (2001) 147.
[13] Y. Yue, A. Gédéon, J.L. Bonardet, N. Melosh, J.B. D'Espinose, J. Fraissard, J. Chem. Soc., Chem. Commun. (1999) 1967.
[14] A. Gédéon, A. Lassoued, J.L. Bonardet, J. Fraissard, Micropor. Mesopor. Mater. 44–45 (2001) 801.
[15] M. Cheng, Z. Wang, K. Sakurai, F. Kumata, T. Saito, T. Komatsu, T. Yashima, Chem. Lett. (1999) 131.
[16] Z. Luan, M. Hartmann, D. Zhao, W. Zhou, L. Kevan, Chem. Mater. 11 (1999) 1621.
[17] T. Yamada, H. Zhou, K. Asai, I. Honma, Mater. Lett. 56 (2002) 93.
[18] P. Van Der Voort, M. Benjelloun, E.F. Vansant, J. Phys. Chem. B 106 (2002) 9027.
[19] C.G. Göltner, B. Smarsly, B. Berton, M. Antonietti, Chem. Mater. 13 (2001) 1617.
[20] F. Gaboriaud, A. Nonat, D. Chaumont, A. Craievich, B. Hanquet, J. Phys. Chem. B 103 (1999) 2091.
[21] Z. Luan, H. He, C.-F. Cheng, W. Zhou, J. Klinowski, J. Phys. Chem. 99 (1995) 1018.
[22] R. López Cordero, A. López Agudo, Appl. Catal. A: Gen. 202 (2000) 23.
[23] R. López Cordero, F.J. Gil Llambias, A. López Agudo, Appl. Catal. 74 (1991) 125.
[24] S. Damyanova, A. Spojakina, K. Jiratova, Appl. Catal. A: Gen. 125 (1995) 257.
[25] R. Thomas, E.M. van Oers, V.H.J. de Beer, J.A. Moulijn, J. Catal. 84 (1983) 275.
[26] B.C. Gates, H. Topsøe, Polyhedron 16 (1997) 3213.
[27] C. Pophal, F. Kameda, K. Hoshino, S. Yoshinaka, K. Segawa, Catal. Today 39 (1997) 21.
[28] S. Yoshinaka, K. Segawa, Catal. Today 45 (1998) 293.